Macromolecules

Article

pubs.acs.org/Macromolecules

Hydrogen-Bonded Polymers with Bent-Shaped Side Chains and Poly(4-vinylpridine) Backbone: Phase Behavior and Thin Film Morphologies

Xiaoshan Liu,[†,‡] Xiaofang Chen,*[,†] Jingkui Wang,[†] Gang Chen,*[,§] and Hailiang Zhang*[,‡]

[†]College of Chemistry, Chemical Engineering and Material Science, Soochow University, Suzhou 215123, P. R. China

[‡]College of Chemistry, Xiangtan University, Xiangtan 411105, P. R. China

[§]Shanghai Institute of Applied Physics, Chinese Academy of Science, Shanghai 201800, P. R. China

Supporting Information

ABSTRACT: We investigate the self-assembly behavior of a series of supramolecular hydrogen bonded polymer complexes P4VP(nCBP)$_x$ in which bent-shaped molecules (nCBP, n = 10,12,14) are attached to a poly(4-vinylpridine) (P4VP) backbone via hydrogen bond interaction in both bulk and thin films. The formation of lamellar and hexagonal columnar (Φ_H) phases are dependent on the blending ratio of nCBP per vinylpridine unit (x), aliphatic tail length (n), and temperature. When increasing the grafting density x, the phase structure of polymer complexes transform from lamellar to Φ_H phase. A nonreversible lamellar to Φ_H phase transition appears in the heating process for P4VP(10CBP)$_x$ with $x \geq 0.4$, P4VP(12CBP)$_x$ with $x \geq 0.3$, and P4VP(14CBP)$_x$ with $x \geq 0.2$. The lamellar and Φ_H phase are oriented parallel to the substrate in the thin film as verified by both GISAXS and AFM.

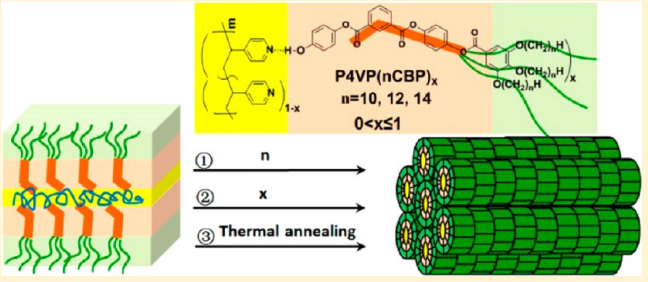

INTRODUCTION

Hydrogen bond interaction exists between H and a highly electronegative atom such as O, F, and N and is one of common noncovalent interactions that are ubiquitous in nature from water to biological systems. The bond energy is larger than the van der Waals interaction but smaller than the covalent bond. With the development of supramolecular chemistry, hydrogen bond interaction has been exploited to enable the incorporation of desired functionality and structural complexity into a variety of supramolecular systems.[1,2]

Supramolecular side chain liquid-crystalline polymers (SCLCPs) and block copolymers (BCPs), in which mesogenic or nonmesogenic amphiphilic small molecules are attached to the polymer backbone as comb-like side chains via hydrogen bonding, have recently gained a lot of attentions because of their fascinating properties in stimuli responsive smart materials.[3−6] In poly(4-vinylpyridine) (P4VP) based homopolymer or BCP supramolecular systems, small molecular additives are generally functionalized with carboxylic or phenolic end groups which can form hydrogen bonds with pyridine side group of P4VP. Because of the relatively weak interaction compared to a covalent bond, the balance between intermolecular interaction and polar−nonploar interaction should be considered to avoid the macroscopic phase separation.[7,8] ten Brinke and Ikkala reported that P4VP-pentadecylphenol (PDP)[9] and P4VP-nonadecylphenol (NDP)[10] complexes can form mesomorphic lamellar structure with the self-assembly mechanism similar to microphase-separation in block copolymers. In addition to flexible linear surfactants additives, rod-like small molecules functionalized with hydroxyl or carboxylic end groups, such as biphenyl derivatives,[11−13] azophenols,[14,15] or azobenzene derivative,[16] and cholesteric derivatives,[17−19] are also able to hydrogen bond with P4VP homopolymer or P4VP based block copolymers, exhibiting lamellar (or smectic)[11,15,17−19] or nematic[13,14,16] mesomorphic structures. When the periodicity of lamellae layer is larger than 4 nm, a self-assembled structure can be directly observed by TEM.[10,17,18]

Furthermore, columnar phase has been found in PVP based hydrogen-bonded supramolecular polymer when dendron-like benzoic acid derivatives are used.[20−22] For example, in P4VP(TDBA)$_x$[21] and PS-b-P4VP(TOB)$_x$[22] complexes when the number of small molecule additives per vinylpyridine repeat unit (x) are larger than 0.6 and 0.5, respectively, stable hexagonal columnar (Φ_H) structures were observed. Below these respective x values, lamellar phases are formed. The grafting density dependent phase transition is similar to P4VP and mesogenic wedge-shaped sulfonic acid complex systems.[23] These studies indicate that various self-assembled ordered nanostructures in supramolecular polymer systems can be obtained through the design and molar fraction of the small molecular additives. Compared with SCLCPs constructed with

Received: April 16, 2014
Revised: June 5, 2014
Published: June 13, 2014

   dx.doi.org/10.1021/ma500794y | Macromolecules 2014, 47, 3917−3925

covalent bonds, in supramolecular LCPs, it is more convenient to modulate the grafting density of side chains by simply controlling the blend ratio of small molecules and polymers. This offers a good opportunity to design and probe novel self-assembled mesomorphic structures based on supramolecular approaches.

Supramolecular block copolymers (BCPs) tend to exhibit complex hierarchically ordered structure-*in*-structure morphologies[24−28] due to phase separation of side groups and BCPs producing ordered nanostructures of variable length scale. In addition, supramolecular BCPs also allow for controlled placement of various functional small molecules, such as semiconductors[29−31] and fluorescent probes,[32] to within a polymer matrix, giving rise to structured materials of novel properties.

We previously reported the synthesis of PS-*b*-P4VP based supramolecular BCP system with a bent-core molecule 1-[4′-(3″,4″,5″ -tridecyloxybenzoyloxy)phenyleneoxycarbonyl]-3-[(4′-hydroxyphenyl)oxycarbonyl]benzene (BP) and the formation of interesting hierarchical supramolecular nanostructures.[33] Hydrogen-bonding interaction exists between phenolic group of BP and pyridine of P4VP, and bilayer smectic LC structure was thus formed within microphase-separated domains of the block copolymer when the molar ratio of BP:VP (vinylpyridine repeating unit) was 0.1 and 0.2. It was shown that a small amount of BP additives tends to dramatically alter the microphase-separated structure and orientation of BCPs upon shearing. In this contribution, we investigate the complexation of P4VP with a series of bent-shaped rigid molecules bearing varying length of aliphatic tails (10CBP, 12CBP, and 14CBP) to afford P4VP(nCBP)$_x$ complexes. x denotes the number of nCBP per vinylpyridine repeat unit. The bent-core is based on the BP structure, and the aliphatic tail varies from 10 to 12 and 14 carbons, respectively (Scheme 1). Self-assembled supramolecular structures of

Scheme 1. Supramolecular P4VP(nCBP)$_x$ Complexes via Hydrogen Bonding

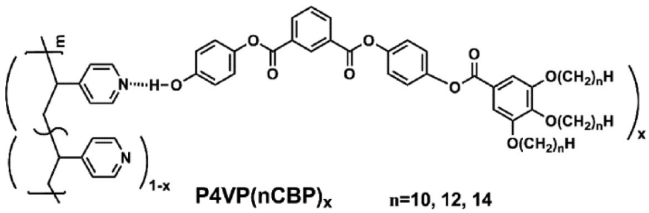

P4VP(nCBP)$_x$ in both bulk and thin films were investigated with a combination of polarized optical microscopy (POM), transmission electron microscopy (TEM), and various X-ray scattering techniques.

EXPERIMENTAL SECTION

Materials. Poly(4-vinylpyridine) (P4VP, weight-average molecular weight, M_w = 5600), was purchased from Polymer Source Inc. and used after purification. Silicon wafers [p-doped, (100)-oriented, 0.45 mm thick, and 100 mm in diameter] were from Guangzhou Semiconductor Materials (Guangzhou, China). nCBP (n = 10,12,14) were synthesized according to the reported literature,[33] and their characterization information were listed in Supporting Information.

Sample Preparation. P4VP(nCBP)$_x$ complexes, where x denotes the number of nCBP per vinylpyridine repeat unit, were prepared by the following procedure. P4VP and nCBP were separately dissolved in chloroform to form 5 wt % solutions and then mixed together in varying proportion to yield homogeneous solutions. After mechanical stirring for about 24 h at room temperature, solvent was allowed to slowly evaporate for 24 h. The obtained samples were then placed in a vacuum oven at 40 °C for another 24 h to remove residual solvent.

Thin Film Preparation. P4VP and nCBP were separately dissolved in chloroform to yield 10 mg/mL solutions and then mixed in different proportion to give homogeneous solutions. The solutions were filtered with 0.2 μm PTFE filters and spin-coated onto freshly cleaned silicon wafers at rotating speed about 1500 rpm for 30 s to produce films of the desired thickness (∼80−90 nm as judged from a spectroscopic ellipsometer). Thin films were thermally annealed for 24 h at different temperatures as required.

Measurements. *Infrared Spectroscopy.* Infrared spectra were obtained using a Bruker VECTOR22 FT-IR spectrometer. Samples were prepared by casting one drop of the chloroform solution (∼10 mg/mL) directly onto potassium bromide crystals. The drying process of FT-IR samples was the same as that mentioned above. The FT-IR measurements were conducted at room temperature.

Differential Scanning Calorimetry. Thermal behavior and phase transition temperatures of all the polymers were observed and obtained using a TA-Q100 DSC instrument. The temperature and heat flow were calibrated using standard materials (indium and zinc) at a cooling and heating rate of 20 °C/min. Samples with a typical mass of about 5 mg were encapsulated in sealed aluminum pans and first melted at 160 °C for 5 min to erase the thermal history. The DSC heating traces were recorded with a rate of 20 °C/min.

Polarized Optical Microscopy. LC textures and birefringence of samples were examined under Leica DM-LM-P polarized optical microscopy (POM) equipped with a Mettler-Toledo FP82HT hot stage. Samples were made by sandwiching the dried polymer powder between a glass slide and a cover glass. Generally, several heating and cooling cycles with controlled rates were carried out to measure the phase transition by detecting the birefringence and morphology change of the sample under POM. Typical LC textures could be formed when heating the sample to its isotropic temperature and then cooling to LC state at a rate of 0.5−1 °C/min. If necessary, thermal annealing at certain LC temperature for several hours was also considered to make the texture more visible.

Small and Wide Angle X-ray Scattering. To identify the phase structures of nCBP and complexed polymers, small and wide-angle X-ray scattering experiments were performed using a high-flux X-ray instrument (SAXSess mc^2, Anton Paar) equipped with Kratky block-collimation system and a GE ID3003 sealed-tube X-ray generator (Cu Kα). The wavelength is 0.1542 nm. Samples were wrapped into aluminum foils and sandwiched in a steel sample holder. The X-ray scattering patterns were recorded in vacuum on an imaging-plate (IP) which extended to high-angle range (the q range covered from 0.06 to 29 nm^{-1}, $q = 4\pi(\sin\theta)/\lambda$, where the λ is the wavelength of 0.1542 nm and 2θ is the scattering angle). The scattering peak positions were calibrated with silver behenate. A temperature control unit (Anton Paar TCS300) in conjunction with the SAXSess mc^2 was utilized to study the structure evolution as a function of temperature.

Synchrotron X-ray Diffraction Measurements. The phase behaviors of sheared samples were studied with X-ray diffraction at the Shanghai Synchrotron Radiation Facility (SSRF, beamline BL14B1). Experiments were carried out with the X-ray wavelength λ = 0.124 nm (E = 10 keV). The size of the primary beam at the sample position was 0.3 mm × 0.3 mm. Diffraction images were collected by a Mar 345 area detector. The sample-to-detector distance was 1.19 m.

Grazing-Incidence Small-Angle X-ray Scattering. The structures of polymer thin films were studied by grazing-incidence small-angle X-ray scattering (GISAXS) by SAXSess mc^2 Anton Paar (Cu Kα radiation, the wavelength was 0.1542 nm) with IP detector 251.5 mm away from the sample in vacuum. Point focused X-ray source with a beam diameter about 0.5 mm incident onto the samples were measured for 30 min with a tilt angle of 0.2° with respect to the primary beam.

Transmission Electron Microscopy. The phase morphologies of complexed samples were observed under transmission electron microscopy (TEM). TEM images were collected on an FEI Tecnai

G-20 transmission electron microscope at an accelerating voltage of 200 kV. The same samples used for SAXS were cut at room temperature by Ultracut UTC microtome (Leica) and collected on 400 mesh copper grids, followed by staining in RuO_4 vapor for 20 min in order to enhance the contrast.

Atomic Force Microscopy. The surface morphologies of complexed polymer thin film were measured on a Multi-Mode Nanoscope V AFM (Bruker Co., Santa Babara, USA). Atomic force microscopy (AFM) images were obtained either on tapping mode with an RTESP (Bruker) silicon cantilever with a nominal spring constant of 40 N/m and a resonance frequency of 300 kHz, or on Peak Force QNM mode with an RFESP (Bruker) silicon cantilever with a nominal spring constant of 3 N/m and a resonance frequency of 75 kHz. The thickness of films on the silicon was determined by a spectroscopic ellipsometer (M-88, J. A. Woollam Co., Inc.) with a detecting angle of 70°. In the modeling of ellipsometry, the software supplied by the instrument producer was used, and Cauchy model was employed to evaluate the films thickness.

RESULTS AND DISCUSSION

1. Phase Structures of nCBP. Phase behavior of nCBP was first characterized by DSC, POM, and SAXS. The results, as shown in Table 1, indicate nCBP tends to enter isotropic state below 100 °C, and the isotropic temperature (T_i) decreases with increasing aliphatic tail length because of the plasticization of soft tails. DSC curves of nCBP can be found in the Supporting Information (Figure S1). Besides the phase transition from LC state to isotropic state, a very weak and broad peak referred to as the crystalline-to-LC state transition around room temperature can be detected as well. Birefringence was observed under POM. The typical fan shaped LC texture with extinction brushes aligned along the polarizers was observed when heating the sample to isotropic temperature and then slowly cooling to LC phase (Figure 1a). Figure 1b shows typical textures when the sample began to exhibit birefringence as cooling from isotropic state. Figure 1C shows mosaic like texture of 14CBP at LC state. The lattice information on LC phase structure of nCBP was obtained by SAXS study. For all nCBPs, three scattering peaks in the low-angle region with a q ratio of $1:\sqrt{3}:2$ were detected, indicating the existence of Φ_H structures, as listed in Table 1. It should be noted that an nCBP molecule is composed of a hydroxyl group, bent-shaped rigid core, and three flexible aliphatic chains. Compared to bent-shaped liquid crystals with a linear aliphatic chain, the topology with the multi chains attached to the phenyl group tends to increase the curvature of aromatic−aliphatic interface, resulting in the predominantly formation of columnar mesomorphic structure. The calculated unit cell dimension is larger than the length of corresponding molecule, which is 3.5 nm for 10CBP, 3.9 nm for 12CBP, and 4.2 nm for 14CBP assuming all stretched aliphatic chains. Thus, the packing model is similar to the hexagonal lattice made of phasmidic, hemiphasmidic, and dendritic molecules with rigid aromatic parts as core and aliphatic parts as shell.[34−36]

Table 1. Phase Behavior of Bent-Core Molecules of nCBP with Data Acquired from DSC and SAXS

		q (1/nm)				
sample	T_i[a] (°C)	(10)	(11)	(20)	a (nm)	structure
10CBP	96	1.25	2.18	2.52	5.80	Φ_H
12CBP	88	1.16	2.03	2.33	6.25	Φ_H
14CBP	84	1.12	1.96	2.23	6.47	Φ_H

[a] T_i refers to isotropic temperature.

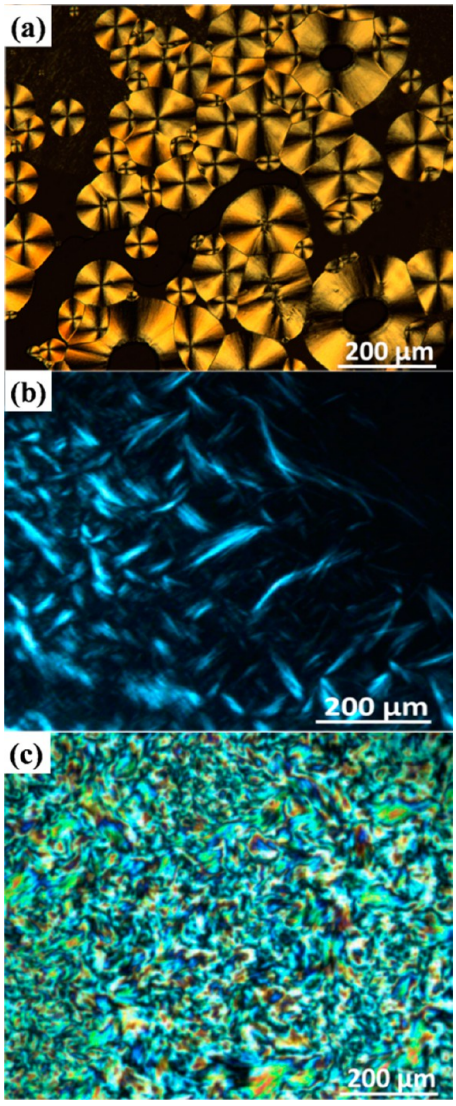

Figure 1. POM images of the texture of nCBP: (a) 10CBP at 40 °C, (b) 12CBP at 90 °C, (c) 14CBP at 70 °C. All pictures were obtained by slowly cooling the sample from isotropic state to LC phase at a rate of 2 °C/min.

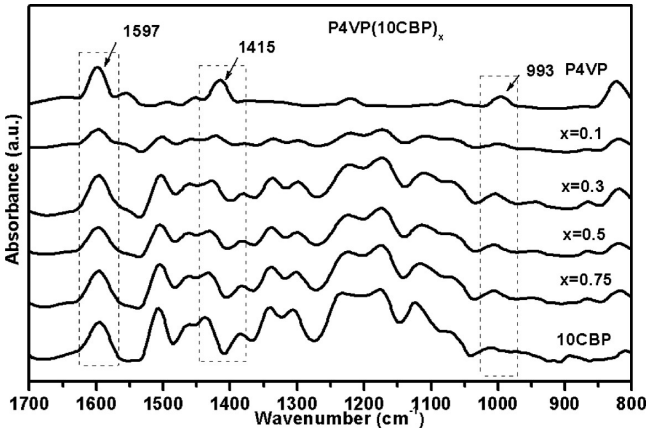

Figure 2. FT-IR spectra of P4VP, 10CBP, and P4VP $(10CBP)_x$ with various 10CBP content (x).

dx.doi.org/10.1021/ma500794y | Macromolecules 2014, 47, 3917−3925

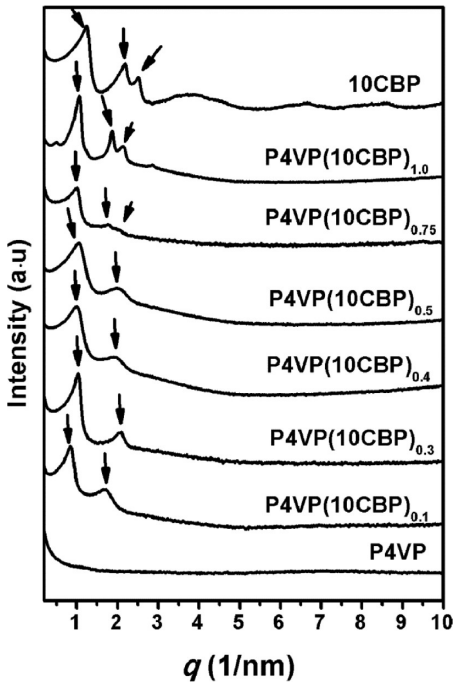

Figure 3. SAXS profiles of P4VP(10CBP)$_x$ complexes recorded at 25 °C.

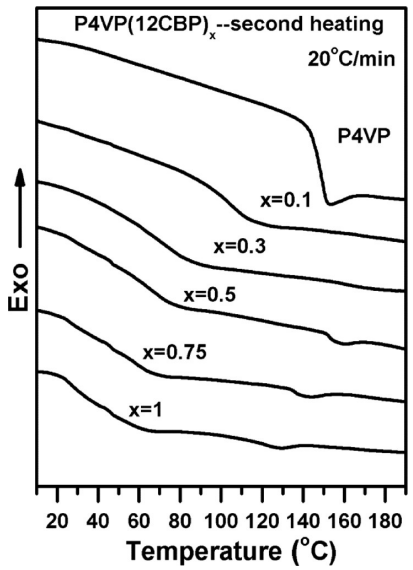

Figure 4. DSC curves of P4VP and P4VP(12CBP)$_x$ during second heating at a rate of 20 °C/min under N_2 atmosphere.

2. Self-Assembly Structure of P4VP (nCBP)$_x$. FT-IR spectroscopy is a well-established and suitable tool for the study of specific interactions in polymer blends[37] and in polymer−surfactant systems.[9] In our work, FT-IR was performed to study the complex formation between P4VP and nCBP. Figure 2 presents the FT-IR spectra of P4VP(10BP)$_x$ complexes together with that of the pure 10CBP and P4VP, respectively. P4VP has absorption bands at 1597, 1415, and 993 cm^{-1}, which are related to those stretching modes of pyridine ring. In agreement with the literature,[9,10,17] when the complex is formed, the absorption bands of pyridine ring at 993 and 1415 cm^{-1} shift to higher wavenumbers in P4VP(10CBP)$_x$ as a consequence of the formation of hydrogen bonding. The absorption band at 1597 cm^{-1} of P4VP is overlapped by the absorption band of benzene ring at 1590 cm^{-1} from 10CBP as the 10CBP content increases. The same situation was observed for the systems with P4VP(12CBP)$_x$ and P4VP(14CBP)$_x$.

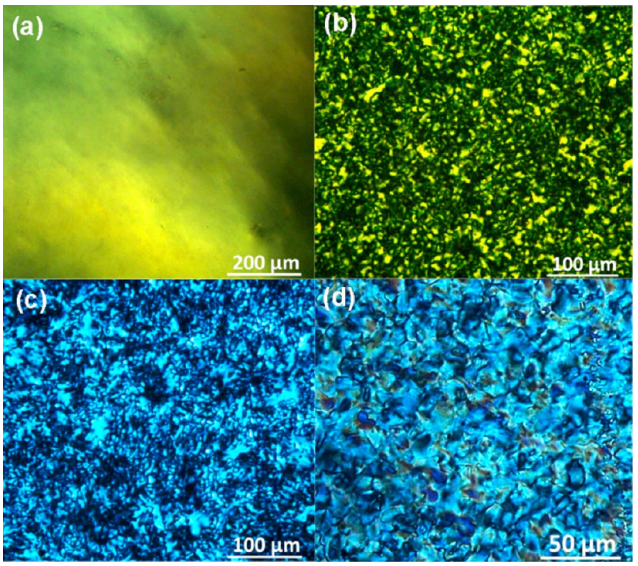

Figure 5. POM images of P4VP(nCBP)$_x$ when cooling from isotropic state to a certain temperature at LC state: (a) P4VP(12CBP)$_{0.1}$ at 30 °C, (b) P4VP(12CBP)$_{0.3}$ at 80 °C, (c) P4VP(12CBP)$_{0.5}$ at 100 °C, and (d) P4VP(10CBP)$_{0.5}$ at 100 °C.

Following the confirmation of hydrogen bonding interaction in the P4VP(nCBP)$_x$ complexes by FT-IR spectroscopy, these self-assembled structures were studied with SAXS technique. Figure 3 shows the SAXS profiles of the as-prepared P4VP(10CBP)$_x$. In contrast to the SAXS curve of crystalline 10CBP at room temperature, there are only several scattering peaks in the low-angle region for P4VP(10CBP)$_x$ complexes revealing their LC nature. Considering the FT-IR results that hydrogen bonds were formed between P4VP and 10CBP, supramolecular LCP were thus obtained successfully with new self-assembled structures. The SAXS of P4VP (10CBP)$_x$, with $x \leq 0.5$, possess two low angle scattering peaks with a q ratio of 1:2, indicating the presence of a lamellar structure. The calculated layer periodicity, based on the SAXS results, decreased gradually from 7.4 nm for x = 0.1−6.0 nm for x = 0.5 with increasing grafting density, which was in agreement with statistical complexation mechanism as reported previously in other P4VP based hydrogen bond systems, such as P4VP-PDP,[9] P4VP-CholHS,[17] and P4VP-TDBA.[21] This can be explained by chain stretching or a decrease of the number of P4VP polymer chains per smectic layer with increasing x. For P4VP(10CBP)$_x$ with a lamellar phase, when $x \leq 0.5$, the layer periodicity was proven to be greater than the calculated molecular length (L = 3.5 nm) for the fully extended unit but slightly smaller than 2L, suggesting a bilayer lamellar structure, which is the same as reported in PS-*b*-P4VP(BP) block copolymer systems.[33]

Interestingly, when further increasing the x up to 0.75 in P4VP(10CBP)$_x$, three diffraction peaks at the low angle region were observed with the q ratio of 1: $\sqrt{3}$:2, indicating the formation of Φ_H phase with the lattice parameter of a = 7.2 nm. Similar composition dependent phase transition was also observed in P4VP(12CBP)$_x$ complexes. When $x < 0.5$, lamellar phase formed, while for $x \geq 0.5$, Φ_H phase appeared instead

dx.doi.org/10.1021/ma500794y | Macromolecules 2014, 47, 3917−3925

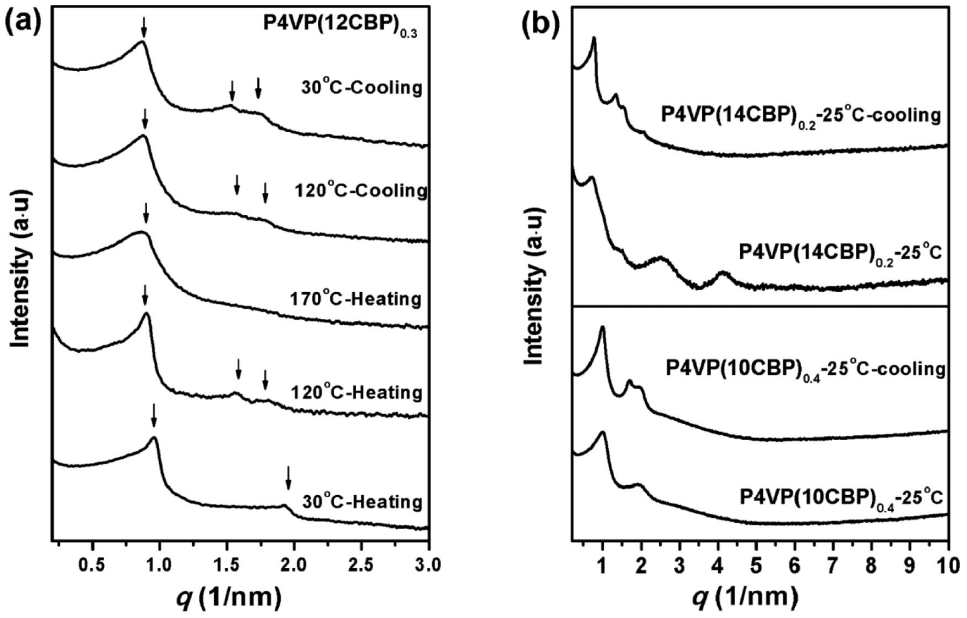

Figure 6. (a) In situ SAXS profiles of P4VP(12CBP)$_{0.3}$ heated from 30 °C (bottom) to 170 °C and subsequently cooled back to 30 °C. (b) SAXS profiles of P4VP(10CBP)$_{0.4}$ and P4VP(14CBP)$_{0.2}$ before and after thermal annealing.

Table 2. Phase Structure Evolution and Corresponding Lattice Parameters of P4VP(nCBP)$_x$ Before and After Thermal Annealing

	before annealing		after annealing	
samples	q^{*a} (nm^{-1})/lattice parameter^b (nm)	phase structure	q^{*a} (nm^{-1})/lattice parameter^b (nm)	phase structure
P4VP(10CBP)$_{0.3}$	1.03/6.10	lam	0.96/6.54	lam
P4VP(10CBP)$_{0.4}$	1.00/6.28	lam	0.99/7.32	Φ_H
P4VP(10CBP)$_{0.5}$	1.05/5.98	lam	1.00/7.25	Φ_H
P4VP(10CBP)$_{0.75}$	1.07/6.84	Φ_H	1.01/7.18	Φ_H
P4VP(12CBP)$_{0.3}$	0.96/6.54	lam	0.87/8.34	Φ_H
P4VP(12CBP)$_{0.5}$	1.00/7.25	Φ_H	0.94/7.71	Φ_H
P4VP(14CBP)$_{0.2}$	0.68/9.23	lam	0.75/9.67	Φ_H
P4VP(14CBP)$_{0.3}$	0.74/8.48	lam	0.85/8.53	Φ_H
P4VP(14CBP)$_{0.5}$	0.77/8.16	lam	0.99/7.32	Φ_H

$^a q^*$ is the scattering vector of the first scattering peak. ^{b}Lattice parameter refer to the periodicity of lamellar structure and a of hexagonal lattice.

(Supporting Information Figure S2). Comparing P4VP(10CBP)$_x$ with P4VP(12CBP)$_x$, we know as the alkyl tail length increases, the columnar phase is favorable and stabilized. In the case of P4VP(14CBP)$_x$, the phase structure is more complicated (Supporting Information Figure S3). When x = 0.1, a lamellar phase was detected by SAXS with the layer thickness up to 10.1 nm, while for $x \geq 0.2$, a highly ordered lamellar or crystalline phase which is different from crystallization of neat 14CBP was detected. This may be due to the crystallization of 14CBP within P4VP matrix. We propose that a complex crystalline system was formed during the solvent evaporation.

As mentioned above, layer like self-assembly structures were most likely found in P4VP based hydrogen bonded supramolecular LCP, whereas in nonmesogenic PDP, or mesogenic rod-like additives, Φ_H was recently found in some systems with dendritic benzoic acid when the grafting density was above a certain value.[21,22] Because the bent-shaped LC mesogenic molecules used in our work are proven to self-assemble into Φ_H structure, the dendritic tails offer the tendency to the formation of columnar phase. So the phenomena are similar to dendritic acid and other dendronized polymers. It is reasonable to observe Φ_H phase in polymer complexes when x is at relatively high value. Meanwhile, when the grafting density is low, lamellar structure is favorable. The grafting density dependent phase transition is quite similar to the reported systems: with increasing grafting density, the lamellar phase first forms and the layer spacing gradually decreases, and finally the system turns into the columnar phase.

3. Thermal Behaviors of P4VP (nCBP)$_x$. The thermal behavior of P4VP(nCBP)$_x$ complexes were first studied by a combination of DSC and POM. Figure 4 shows a series of second heating DSC curves of P4VP(12CBP)$_x$ at a rate of 20 °C/min under nitrogen atmosphere after eliminating the thermal history. First of all, the DSC results show that the glass transition temperature (T_g) of P4VP(12CBP)$_x$ complex decreases with increasing the molar ratio of 12CBP(x) to the repeating unit of P4VP, which is due to plasticization by the bent-shaped supramolecular side chains. Besides T_g, an endothermic peak could be observed for $x \geq 0.5$, associated with phase transition from LC state to isotropic state. The transition temperature is above 100 °C, which is different form the phase behavior of 12CBP, indicating the complexation formed between P4VP and 12CBP. Similar DSC curves of P4VP(10CBP)$_x$ are also observed (Supporting Information Figure S4). According to POM study, all complexes show birefringence at the room temperature. When cooling the samples from isotropic state to LC state, the complexes with lower x just exhibit weak birefringence under POM (Figure 5a). Parts b and c of Figure 5 show schlieren texture of P4VP(12BP)$_{0.3}$ and mosaic like texture P4VP(12BP)$_{0.5}$, respectively. Similar POM pictures of P4VP(10CBP)$_{0.5}$ are observed in Figure 5d.

Phase behavior of P4VP(nCBP)$_x$ were further studied by one-dimensional (1D) and two-dimensional (2D) SAXS at

dx.doi.org/10.1021/ma500794y | Macromolecules 2014, 47, 3917−3925

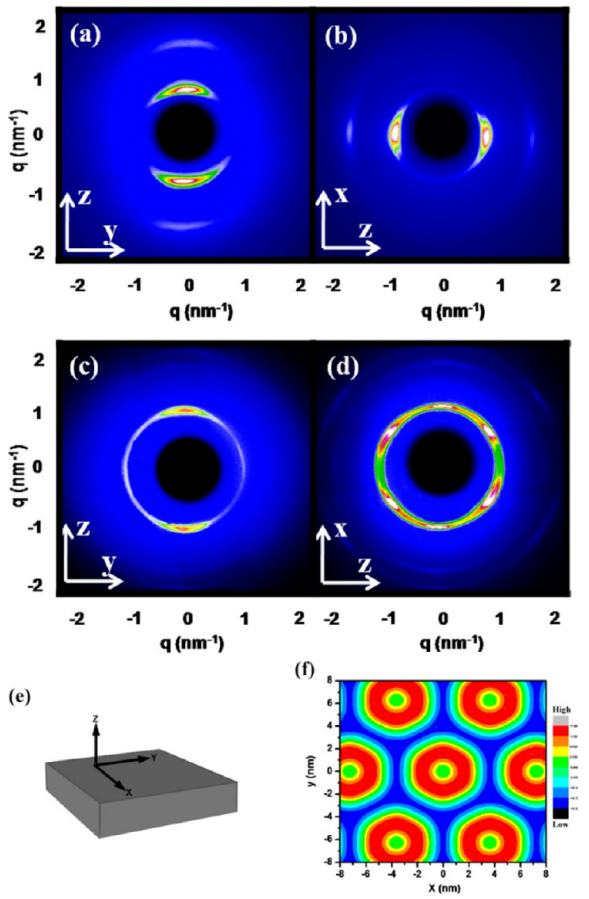

Figure 7. 2D XRD pattern of P4VP(10CBP)$_{0.1}$ sample with X-ray beam perpendicular and parallel to the shear direction (a,b), respectively. (c) and (d) are 2D XRD patterns of P4VP(10CBP)$_{0.75}$ with X-ray beam perpendicular and parallel to the shear direction, respectively. (e) Schematic illustration of shear geometry. x is shear direction, y is shear vorticity direction, and z is shear gradient direction. (f) Relative electron density map of hexagonal lattice of P4VP(10CBP)$_{0.75}$.

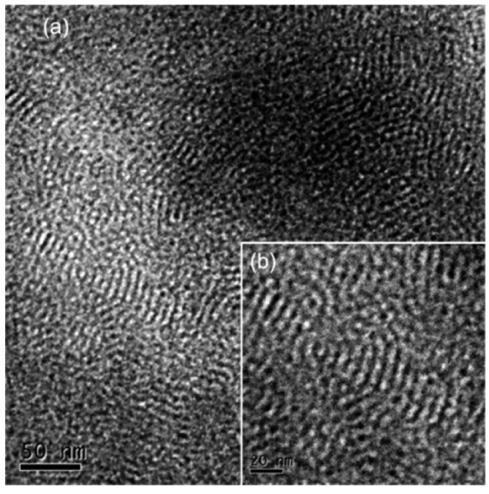

Figure 8. TEM pictures of P4VP(10CBP)$_{0.3}$(a) and inset (b) of corresponding TEM image.

elevated temperatures. For an example, when x < 0.3, P4VP(12CBP)$_x$ exhibit lamellar phase structure upon heating cycle and keep the same structure when cooling from isotropic state. Interestingly, when x = 0.3, the as-prepared polymer complex exhibit lamellar phase structure at the room temperature (Figure 6), while a nonreversible order−order transition (OOT) from lamellar to Φ_H phase were detected upon heating by SAXS as shown in Figure 5. As can be seen, at room temperature the SAXS curve shows two scattering peaks located at q = 0.96 and 1.92 nm^{-1} corresponding to a lamellar structure with a periodicity of 6.54 nm. As the temperature increases to 120 °C, three scattering peaks located at q = 0.90, 1.56, and 1.80 nm^{-1} appear with the q ratio of 1:$\sqrt{3}$:2, indicating the phase structure changed from lamellar to Φ_H phase with a = 8.1 nm. When heating is continued to 170 °C where P4VP(12CBP)$_{0.3}$ is in its isotropic state, only one broad peak exists, which is attributed to the concentration fluctuations in an homogeneous state as reported before.[9] Upon the cooling cycle from 170 °C to the room temperature, Φ_H structure appeared again at a temperature of 120 °C and kept to the room temperature. In situ 2D XRD study of P4VP(12CBP)$_{0.3}$ at different temperatures in Supporting Information Figure S5 also gives the same evidence about the nonreversible OOT. Moreover, identical nonreversible phase transition was also observed in the P4VP(10CBP)$_x$ and P4VP(14CBP)$_x$ but with the different threshold values of x, for P4VP(10CBP)$_x$, when $x \geq 0.4$, and for P4VP(14CBP)$_x$, when $x \geq 0.2$, respectively. Figure 6b shows SAXS profiles of P4VP(10CBP)$_{0.4}$ and P4VP(14CBP)$_{0.2}$ before and after heating and cooling cycles, indicating the different phase structure appears after thermal annealing. Such nonreversible OOT has not been observed in other hydrogen-bonded polymer systems. Xu et al.[19] reported a nonreversible order−order transition in a block copolymer supramolecular system composed of PS-*b*-P4VP and 3-hydroxyphenyl cholesteryl succinate (ChHP). The macrophase separation of the ChHP molecules takes place after thermal annealing, which induces the BCP's morphological transition. In our case, we did not observe small molecules diffused out of polymer matrix after thermal annealing. So the OOT is assumed to the self-assembly structure transformation from metastable state to thermal stable one during the thermal annealing. Because the small molecules with dendron-like aliphatic tails tend to form columnar phase, the thermal stable lamellar phase can only exist when the x of P4VP(nCBP)$_x$ complexes is low. By increasing x to a critical value, the volume fraction of nonpolar part increases to some extent that the lamellar structure becomes a metastable state. When heating the sample obtained during solvent vaporing, the curvature of dendritic aliphatic−aromatic interface increases, which is favorable to columnar phase formation. The threshold value of x for complexes to appear nonreversible OOT decreases with increasing the aliphatic chain length, which further supported our assumption. The other possible reason is after thermal annealing, the distribution of small molecules attached to the polymer backbone might be rearranged because of the thermal sensitive feature of hydrogen bonding interaction between polymer chain and small molecule additives. Table 2 shows the phase information on a list of some complexes before and after thermal annealing. The lattice parameter of Φ_H phase decreases slightly with increasing x, indicating that increasing the grafting density can force the P4VP polymer backbone adopt more stretched conformation.

2D SAXS experiments were carried out to further study the orientation of lamellar and structure of macroscopically oriented samples were obtained by mechanical shear at the mesophase temperature. Figure 6e shows the schematic

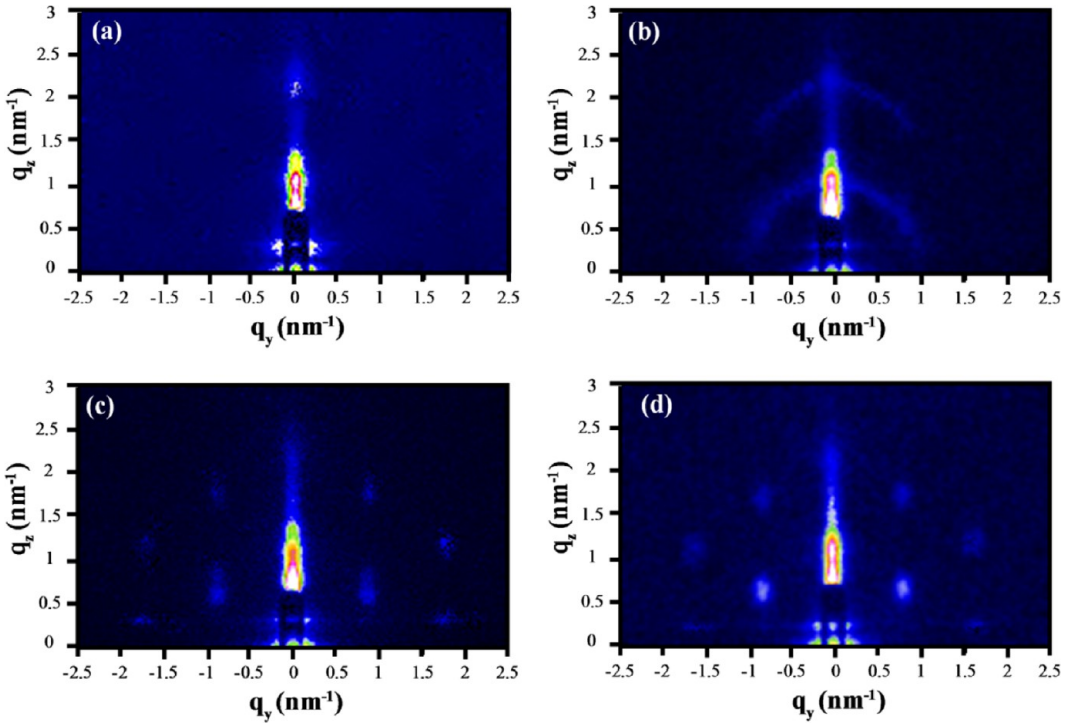

Figure 9. GISAXS patterns of thin films obtained at incident angle $\alpha_i = 0.20°$ (a) P4VP(10CBP)$_{0.3}$ ~ 92 nm in thickness, after thermal annealing at 100 °C for 24 h, (b) P4VP(10CBP)$_{0.4}$ ~90 nm in thickness, after thermal annealing at 100 °C for 24 h, (c) P4VP(10CBP)$_{0.75}$ ~ 86 nm in thickness, after thermal annealing at 75 °C for 24 h, and (d) P4VP(12CBP)$_{0.5}$ ~ 85 nm in thickness, after thermal annealing at 90 °C for 24 h.

illustration of shear geometry, with x as shear direction and z as shear gradient. The 2D SAXS patterns recorded at room temperature with the X-ray incident beam parallel to x, y, and z directions, respectively. Parts a and b of Figure 7b show 2D SAXS patterns of P4VP(10CBP)$_{0.1}$ when X-ray incident beam is parallel to y and x direction, respectively, and sample placed with the shear direction along the equator. Both SAXS patterns show two pairs of sharp diffractions arcs near the beam stop appear on the meridian. Careful analysis shows that the scattering vector ratio of the diffractions in the 2D SAXS followed 1:2, suggesting a lamellar structure, which agrees with the result from 1D SAXS. The position of diffraction arcs indicates that after mechanical shearing lamellar structure is parallel to the shear direction. Parts c and d of Figure 7 show the 2D SAXS pattern of P4VP(10CBP)$_{0.75}$. When X-ray incident beam is parallel to y direction, a pair of diffraction arc on the equator appears (Figure 7c), indicating the cylinders adopt parallel alignment along the shear direction. Meanwhile, when X-ray incident beam is parallel to the x direction, diffraction arcs with 6-fold symmetry is observed (Figure 7d), representing a hexagonal close packed cylinder structure. The reconstructed relative electron density map[38] of hexagonal lattice of P4VP(10CBP)$_{0.75}$ is presented in Figure 6f. The core of column, which displays green and yellow color indicating intermediate electron density, should be filled with P4VP backbone. The hexagonal lattice parameter of 10CBP and P4VP(10CBP)$_{0.75}$ is 5.80 and 7.19 nm, respectively. Assuming the similar packing model, the diameter of P4VP backbone could be estimated as 1.4 nm, which is quite close to the size of column core in the electron density map. Away from the core area, the electron density increases with red color, which belongs to the rigid part of side chains. The area with the lowest electron density (blue colored) certainly belongs to aliphatic tails. Core−shell-like cylinders incorporating P4VP backbone and bent shaped side chain are thus formed which self-assemble into Φ_H phase.

On the basis of the combination of POM, DSC, and SAXS results, obviously P4VP(nCBP)$_x$ complexes could self-assemble into lamellar and Φ_H phase depending on the values of x and n. Because of relatively large mesogenic side chain, lattice parameter of phase structures are larger than 6 nm, which is accessible by TEM. Figure 8 shows the TEM image of P4VP(10CBP)$_{0.3}$, from which randomly distributed lamellae could be seen, and the lamellae has a periodicity of ~6 nm.

4. Phase Structures in Thin Films. We further investigate their thin film morphologies and structure orientation within the films. Two experimental techniques were employed in this work to investigate the structural evolution of the system. The surface morphologies of these films are revealed with AFM. Meanwhile, GISAXS is utilized to probe the order and interior structure. Figure 9a shows the GISAXS pattern of P4VP(10CBP)$_{0.3}$ film at an incident angle of 0.2°; two diffraction spots are seen in the q_z direction, indicating that the lamellar structure formed in the film have a good orientation with the layer parallel to the substrate. The q_z scan at $q_y = 0$ nm^{-1} shows the first diffraction spot at $q_z = 1.03$ nm^{-1}, which is consistent with a period of ~6.1 nm in bulk. Figure 9b shows the GISAXS pattern of P4VP(10CBP)$_{0.4}$ film which appears to be a combination of spot-like pattern and diffraction rings. Because the bulk sample of P4VP(10CBP)$_{0.4}$ undergoes a nonreversible lamellar to Φ_H structure transition after thermal annealing, the thin film morphology appears a coexistence of two mesophases and not be able to form uniform orientation. Parts c and d Figure 9 are GISAXS patterns of P4VP(10CBP)$_{0.75}$ and P4VP(12CBP)$_{0.5}$, showing nice orientation of the columnar phase with the cylinder aligned parallel within the film. Corresponding AFM images of P4VP(12CBP)$_{0.5}$ and P4VP(10CBP)$_{0.75}$ thin films of ~86 nm in thickness are shown in

dx.doi.org/10.1021/ma500794y | Macromolecules 2014, 47, 3917−3925

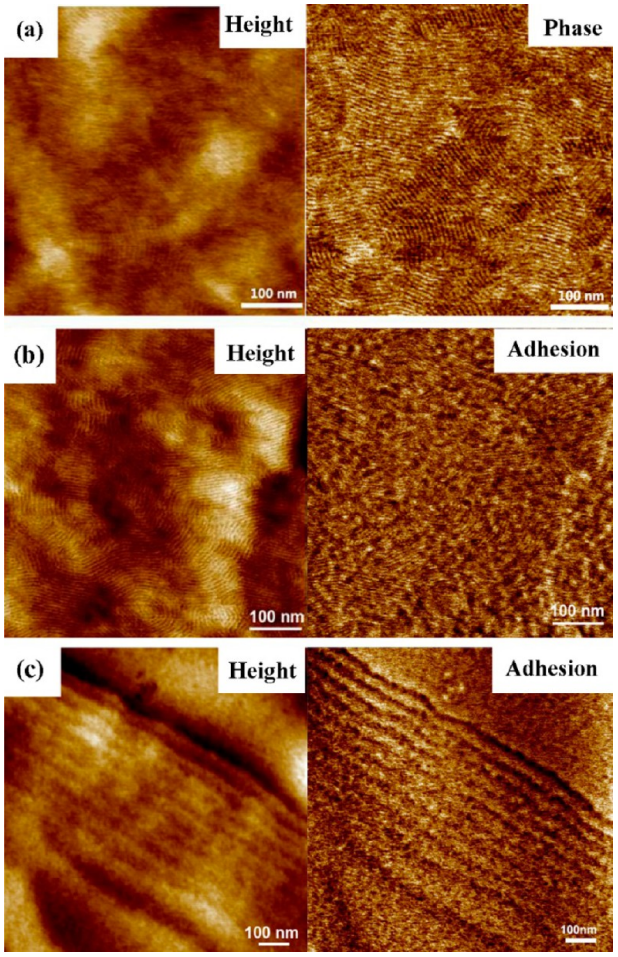

Figure 10. (a) AFM height and phase image of P4VP(12CBP)$_{0.5}$ thin film, ~85 nm in thickness, after thermal annealing at 90 °C for 24 h. The z scale is 4.4 nm for height and 3.4° for phase. (b) AFM height and adhesion image of P4VP(10CBP)$_{0.75}$ thin film, ~86 nm in thickness, after thermal annealing at 75 °C for 24 h. The z scale is 5 nm for height and 5 mV for adhesion. (c) AFM height and adhesion image of P4VP(10CBP)$_{0.3}$ thin film, ~92 nm in thickness, after thermal annealing at 100 °C for 24 h. The z scale is 10 nm for height and 6.8 mV for adhesion.

parts a and b of Figure 10. The films show fingerprint-like patterns composed of parallel strips on the surface, which is a typical morphology of columnar phase on the thin film when cylinders are parallel to the surface. Similar morphology has been frequently observed in some block copolymer thin films with columnar microphase-separated structures.[39] The parallel orientation of hexagonal packed cylinders is in good agreement with the orientation determined by GISAXS.[40] The orientation of cylinders in thin films can be parallel or perpendicular to the surface according to the surface energy, thin film thickness, and other processing treatments.[41] As discussed above, the Φ_H structure in bulk P4VP(nCBP)$_x$ is constructed with supramolecular core−shell like cylinders composed of P4VP chain as the core and hydrogen bonded side chains as the shell. So in thin films, the polymer chain within the cylinder tends to lie down in the thin film rather than perpendicular to the surface after thermal annealing. On the basis of the polymer chain orientation, parallel orientation of cylinders is thermodynamically preferred. Meanwhile, P4VP has strong interaction with silicon oxide surface of the substrate,[42] which further favors the parallel orientation in thin films. The interaction between the polymer complex and the substrate influences the lamellar structure's orientation as well. AFM morphology of the P4VP(10CBP)$_{0.3}$ thin film is featureless, and only layer-like morphology could be detected near the edge of the thin film (Figure 10c), which indicates the parallel orientation of lamellar structure to the substrate within the film, consistent with the GISAXS result. The feasible formation of sub-10 nm regular pattern in this supramolecular system provides an opportunity to further tailor the surface pattern and properties of thin films via different processing techniques.

CONCLUSIONS

Supramolecular hydrogen bonded liquid crystalline polymer complexes P4VP(nCBP)$_x$ were prepared, and their self-assembly structures in bulk and thin films were characterized by a combination of DSC, POM, and SAXS techniques. Lamellar and Φ_H phases were observed in this system, and their formation depends on the grafting density, aliphatic tail length, temperature, and thermal history. When increasing x, the phase structure of polymer complexes transform from lamellar to Φ_H phase and the threshold value of x dependent phase transition decreases with increasing the tail length. A nonreversible lamellar to Φ_H phase transition appears in the heating process for P4VP(10CBP)$_x$ with $x \geq 0.4$, P4VP(12CBP)$_x$ with $x \geq 0.3$, and P4VP(14CBP)$_x$ with $x \geq 0.2$. Because of the relatively large structure periodicity around 6−10 nm, the phase morphology could be observed under TEM and AFM. GISAXS revealed that in thin film the phase structure spontaneously oriented parallel to the substrate. Further investigation about their thin film properties and other complex hierarchical self-assembly structures in block copolymer systems are currently in progress.

ASSOCIATED CONTENT

Supporting Information

Characterization of small molecules nCBP (n = 10, 12, 14), including ^{1}HNMR, EA, and DSC, SAXS of P4VP(12CBP)$_x$ and P4VP(14CBP)$_x$, DSC of P4VP(10CBP)$_x$, 2D SAXS of P4VP(12CBP)$_{0.3}$. This material is available free of charge via the Internet at http://pubs.acs.org.

AUTHOR INFORMATION

Corresponding Authors

*X.-F.C.: E-mail, xfchen75@suda.edu.cn.
*G.C.: E-mail, chengang@sinap.ac.cn.
*H.-L.Z.: E-mail, hailiangzhang@xtu.edu.cn.

Notes

The authors declare no competing financial interest.

ACKNOWLEDGMENTS

This work was supported by the National Natural Science Foundation of China (21174003). We also thank Dr. Shuang Yang (Peking University) for help in electron density map calculation.

REFERENCES

(1) Lenh, J. M. *Angew. Chem., Int. Ed.* **1988**, *27*, 89−112.
(2) Whitesides, G. M.; Mathaias, J. P.; Seto, C. T. *Science* **1991**, *254*, 1312−1319.
(3) Kato, T.; Kihara, H.; Ujiie, S.; Uryu, T.; Frechet, J. M. J. *Macromolecules* **1996**, *29*, 8734−8739.
(4) Pollino, J. M.; Weck, M. *Chem. Soc. Rev.* **2005**, *34*, 193−207.

(5) ten Brinke, G.; Ruokolainen, J.; Ikkala, O. *Adv. Polym. Sci.* **2007**, *207*, 113−177.
(6) Hammond, M. R.; Mezzenga, R. *Soft Matter* **2008**, *4*, 952−961.
(7) Ruokolainen, J.; Torkkeli, M.; Serimaa, R.; Vahvaselka, S.; Saariaho, M.; tenBrinke, G.; Ikkala, O. *Macromolecules* **1996**, *29*, 6621−6628.
(8) Wu, S.; Bubeck, C. *Macromolecules* **2013**, *46* (9), 3512−3518.
(9) Ruokolainen, J.; ten Brinke, G.; Ikkala, A. O.; Torkkeli, M.; Serimaa, R. *Macromolecules* **1996**, *29*, 3409−3415.
(10) Ruokolainen, J.; Tanner, J.; Ikkala, O.; ten Brinke, G.; Thomas, E. L. *Macromolecules* **1998**, *31*, 3532−3536.
(11) Bazuin, C. G.; Brandys, F. A. *Chem. Mater.* **1992**, *4*, 970−972.
(12) Brandys, F. A.; Bazuin, C. G. *Chem. Mater.* **1996**, *8*, 83−92.
(13) Han, X. G.; Zhang, S. B.; Shanks, R. A.; Pavel, D. *React. Funct. Polym.* **2008**, *68*, 1097−1102.
(14) Wu, X. D.; Zhang, G. L.; Zhang, H. Z. *Macromol. Chem. Phys.* **1998**, *199*, 2101−2105.
(15) de Wit, J.; van Ekenstein, G. A.; Polushkin, E.; Kvashnina, K.; Bras, W.; Ikkala, O.; ten Brinke, G. *Macromolecules* **2008**, *41*, 4200−4204.
(16) del Barrio, J.; Blasco, E.; Oriol, L.; Alcala, R.; Sanchez-Somolinos, C. *J.Polym. Sci., Part A: Polym. Chem.* **2013**, *51* (8), 1716−1725.
(17) Korhonen, J. T.; Verho, T.; Rannou, P.; Ikkala, O. *Macromolecules* **2010**, *43*, 1507−1514.
(18) Soininen, A. J.; Tanionou, I.; ten Brummelhuis, N.; Schlaad, H.; Hadjichristidis, N.; Ikkala, O.; Raula, J.; Mezzenga, R.; Ruokolainen, J. *Macromolecules* **2012**, *45* (17), 7091−7097.
(19) Bai, P.; Kim, M. I.; Xu, T. *Macromolecules* **2013**, *46*, 5531−5537.
(20) Vera, F.; Almuzara, C.; Orera, I.; Barbera, J.; Oriol, L.; Serrano, J. L.; Sierra, T. *J. Polym. Sci. Part A: Polym. Chem.* **2008**, *46*, 5528−5541.
(21) Wang, S. J.; Xu, Y. S.; Yang, S.; Chen, E. Q. *Macromolecules* **2012**, *45*, 8760−8769.
(22) Chuang, W. T.; Sheu, H. S.; Jeng, U. S.; Wu, H. H.; Hong, P. D.; Lee, J. J. *Chem. Mater.* **2009**, *21*, 975−978.
(23) Zhu, X. M.; Beginn, U.; Moller, M.; Gearba, R. I.; Anokhin, D. V.; Ivanov, D. A. *J. Am. Chem. Soc.* **2006**, *128*, 16928−16937.
(24) Ruokolainen, J.; ten Brinke, G.; Ikkala, O. *Adv. Mater.* **1999**, *11*, 777−780.
(25) Ruokolainen, J.; Saariaho, M.; Ikkala, O.; ten Brinke, G.; Thomas, E. L.; Torkkeli, M.; Serimaa, R. *Macromolecules* **1999**, *32*, 1152−1158.
(26) Ruokolainen, J.; Makinen, R.; Torkkeli, M.; Makela, T.; Serimaa, R.; ten Brinke, G.; Ikkala, O. *Science* **1998**, *280* (5363), 557−560.
(27) Ikkala, O.; ten Brinke, G. *Science* **2002**, *295* (5564), 2407−2409.
(28) ten Brinke, G.; Ikkala, O. *Chem. Rec.* **2004**, *4* (4), 219−230.
(29) Rancatore, B. J.; Mauldin, C. E.; Tung, S.-H.; Wang, C.; Hexemer, A.; Strzalka, J.; Frechet, J. M. J.; Xu, T. *ACS Nano* **2010**, *4*, 2721−2729.
(30) Rancatore, B. J.; Mauldin, C. E.; Frechet, J. M. J.; Xu, T. *Macromolecules* **2012**, *45*, 8292−8299.
(31) Narayan, R.; Kumar, P.; Narayan, K. S.; Asha, S. K. *Adv. Funct. Mater.* **2013**, *23*, 2033−2043.
(32) Kuila, B. K.; Chakraborty, C.; Malik, S. A. *Macromolecules* **2013**, *46*, 484−492.
(33) Tenneti, K. K.; Chen, X. F.; Li, C. Y.; Wan, X. H.; Fan, X. H.; Zhou, Q. F.; Rong, L. X.; Hsiao, B. S. *Macromolecules* **2007**, *40*, 5095−5102.
(34) Nguyen, H.-T.; Destrade, C.; Malthête, J. *Adv. Mater.* **1997**, *9*, 375−388.
(35) Balagurusamy, V. S. K.; Ungar, G.; Percec, V.; Johansson, G. *J. Am. Chem. Soc.* **1997**, *119* (7), 1539−1555.
(36) Rosen, B. M.; Wilson, C. J.; Wilson, D. A.; Peterca, M.; Imam, M. R.; Percec, V. *Chem. Rev.* **2009**, *109* (11), 6275−6540.
(37) Painter, P. C.; Graf, J. F.; Coleman, M. M. *Macromolecules* **1991**, *24* (20), 5630−5638.
(38) Zheng, J. F.; Liu, X.; Chen, X. F.; Ren, X. K.; Yang, S.; Chen, E. Q. *ACS Macro Lett.* **2012**, *1*, 641−645.
(39) van Dijk, M. A.; van den Berg, R. *Macromolecules* **1995**, *28*, 6773−6778.
(40) Chao, K. J.; Liu, P.-H.; Huang, K.-Y. *C.R. Chimie* **2005**, *8*, 727−739.
(41) Hamley, I. W. *Prog. Polym. Sci.* **2009**, *34* (11), 1161−1210.
(42) Liu, Y.; Zhao, W.; Zheng, X.; King, A.; Singh, A.; Rafailovich, M. H.; Sokolov, J.; Dai, K. H.; Kramer, E. J.; Schwarz, S. A.; Gebizlioglu, O.; Sinha, S. K. *Macromolecules* **1994**, *27* (14), 4000−4010.